Inorganic Chemistry

Article

pubs.acs.org/IC

# Binuclear Cyclopentadienylmetal Methylene Sulfur Dioxide Complexes of Rhodium and Iridium Related to a Photochromic Metal Dithionite Complex

Dongsheng Rong,[†,§] Shida Gong,[†,‡,§] Chaoyang Wang,[†] Qiong Luo,[*,†] Qian-shu Li,[†] Yaoming Xie,[⊥] R. Bruce King,[*,†,⊥] and Henry F. Schaefer[⊥]

[†]MOE Key Laboratory of Theoretical Environmental Chemistry, Center for Computational Quantum Chemistry, South China Normal University, Guangzhou 510631, P. R. China

[‡]School of Chemistry and Chemical Engineering, Qingdao University, Qingdao 266071, P. R. China

[⊥]Department of Chemistry and Center for Computational Chemistry, University of Georgia, Athens, Georgia 30602, United States

Supporting Information

**ABSTRACT:** The photochromic dithionite complex $Cp^*_2Rh_2(\mu\text{-}CH_2)_2(\mu\text{-}O_2SSO_2)$ ($Cp^* = \eta^5\text{-}Me_5C_5$) is of interest because it undergoes an unusual fully reversible unimolecular photochemical rearrangement to the isodithionite complex $Cp^*_2Rh_2(\mu\text{-}CH_2)_2(\mu\text{-}O_2SOSO)$. In order to obtain more insight into these systems, a comprehensive density functional theory study has been carried out on isomeric $Cp_2M_2(CH_2)_2(SO_2)_2$ (M = Rh, Ir) derivatives. The experimentally observed rhodium complexes with coupled sulfur dioxide ($SO_2$) units to give dithionite or isodithionite ligands are surprisingly high-energy kinetic isomers in our analysis, reflecting the need for dithionite rather than $SO_2$ for their synthesis. Many isomeric structures containing two separate $SO_2$ ligands are found to lie at lower energies than these dithionite and isodithionite complexes. In the lowest-energy $Cp_2M_2(CH_2)_2(SO_2)_2$ isomers, the two methylene groups couple to form an ethylene ligand that can be either terminal or bridging. In slightly higher energy structures, a formal hydrogen shift is predicted to occur within the ethylene ligand to give a methylcarbene $CH_3CH$ ligand. Isomers with a bridging methylcarbene ligand are energetically preferred over isomers with a terminal methylcarbene ligand. Generation of the lower-energy $Cp_2Rh_2(CH_2)_2(SO_2)_2$ isomers containing separate $SO_2$ ligands should be achievable through reactions of $SO_2$ with more highly reduced cyclopentadienylrhodium methylene complexes such as $Cp^*_2Rh_2(\mu\text{-}CH_2)_2$.

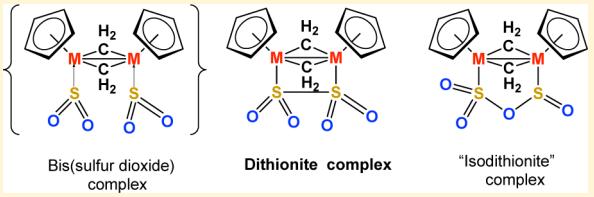


## 1. INTRODUCTION

Sulfur dioxide ($SO_2$) is of interest as a very versatile amphoteric ligand behaving as either a Lewis acid or base depending upon the circumstances.[1,2] As a Lewis base in transition-metal chemistry, $SO_2$ can bind to a metal through its sulfur atom, through an oxygen atom, or through an S═O $\pi$ bond (Figure 1).[3,4] In addition, $SO_2$ can behave as a mild oxidant or reductant as well as an oxygen donor or acceptor. Reductive coupling of $SO_2$ generates the dithionite dianion $S_2O_4^{2-}$. Normally dithionite is synthesized by the reduction of a sulfite ion with zinc dust or by the reduction of $NaHSO_3$ with sodium borohydride. The formation of dithionite from the reduction of sulfur dioxide or sulfites involves coupling of the sulfur dioxide radical anion $SO_2^-$. The structure of the dithionite anion $[O_2SSO_2]^{2-}$ has the two $SO_2$ units joined by a relatively long 2.39 Å S−S bond.[5,6]

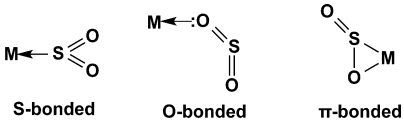


**Figure 1.** Modes of bonding an $SO_2$ ligand to a transition-metal atom.

The dithionite anion only rarely serves as a ligand in transition-metal chemistry. However, it functions as a chelating ligand through its sulfur atoms in the cyclopentadienylrhodium complexes $Cp_2Rh_2(\mu\text{-}CH_2)_2(\mu\text{-}S_2O_4)$ [$Cp = \eta^5\text{-}Me_5C_5$ (=Cp*) or $\eta^5\text{-}EtMe_4C_5$ (=$Cp^{Et}$); Figure 2].[7−10] These species exhibit an

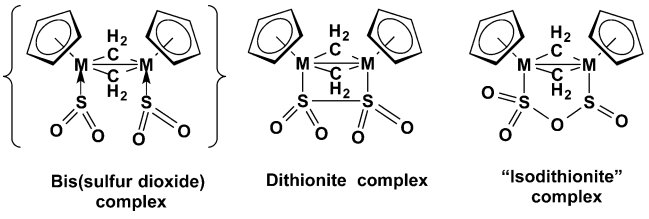


**Figure 2.** Different bonding modes of an $S_2O_4$ unit in a $Cp_2M_2(\mu\text{-}CH_2)_2(S_2O_4)$ (M = Rh, Ir) compound. Substituents on the cyclopentadienyl rings are omitted for clarity.

**Received:** August 10, 2017
**Published:** November 15, 2017






DOI: 10.1021/acs.inorgchem.7b02064
*Inorg. Chem.* 2017, 56, 14486−14493

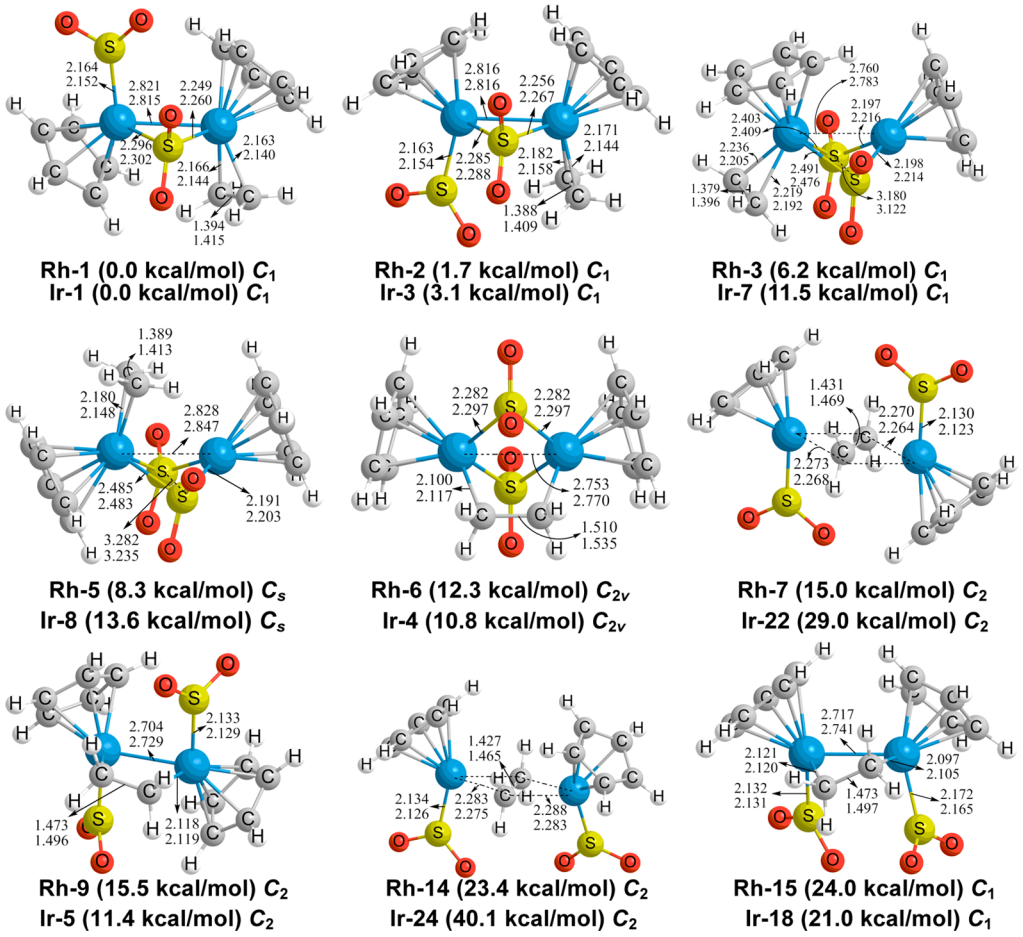


**Figure 3.** $Cp_2M_2(SO_2)_2(CH_2)_2$ (M = Rh, Ir) structures with the methylene groups coupled to give coordinated ethylene optimized by the $\omega$B97X-D method. The distances (in Å) for M = Rh are on the top, and those for M = Ir are on the bottom.

unusual type of photochromism involving rearrangement of the coordinated dithionite ligand $[O_2SSO_2]^{2-}$ into an isomeric $[O_2SOSO]^{2-}$ "isodithionite" ligand in which a terminal oxygen atom is inserted into the S−S bond of the original dithionite ligand. Such an "isodithionite" ligand is unknown in the uncomplexed form. A driving force behind this reaction would be expansion of the four-membered $Rh_2S_2$ chelate ring in the dithionite complex into a less strained five-membered $Rh_2S_2O$ chelate ring in the isodithionite complex without apparently disturbing the two Rh−S bonds in these complexes. Experimentally, the red-brown dithionite complex $Cp^*_2Rh_2(\mu\text{-}CH_2)_2(\mu\text{-}O_2SSO_2)$ converts to the yellow-orange isodithionite complex $Cp^*_2Rh(\mu\text{-}CH_2)_2(\mu\text{-}O_2SOSO)$ upon exposure to the light of a xenon lamp, thereby indicating a photochromic system. The isodithionite complex reverts quantitatively back to the dithionite complex in the dark for 3 weeks at room temperature. Both isomers are stable enough for structure determination by X-ray crystallography. The S−S bond length of 2.330 Å in the dirhodium dithionite complex is significantly shorter than the 2.39 Å S−S bond in the free dithionite dianion possibly because of Coulombic repulsion between the sulfur atoms in the free dianion. The Rh−Rh distance of 2.622 Å in the dithionite complex undergoes essentially no change to 2.626 Å in the isodithionite complex.

The dithionite complex $Cp^*_2Rh_2(\mu\text{-}CH_2)_2(\mu\text{-}S_2O_4)$ is obtained by the reaction of $Cp^*_2Rh_2(\mu\text{-}CH_2)_2Cl_2$ with sodium dithionite in methanol.[7] However, it can also be formally derived from the rearrangement of a hypothetical $SO_2$ complex $Cp^*_2Rh_2(\mu\text{-}CH_2)_2(SO_2)_2$ by the formation of a S−S bond. This $SO_2$ complex is of interest because it contains two types of ligands that can dimerize on the metal (M) atom. Thus, the two methylene ligands can dimerize to form coordinated ethylene, and/or the two $SO_2$ ligands can dimerize to form coordinated dithionite. In order to obtain more information on this type of system, we have used density functional theory (DFT) to explore the geometries and relative energies of $Cp_2M_2(\mu\text{-}CH_2)_2(SO_2)_2$ (M = Rh, Ir) and their isomers with coupled $CH_2$ and/or $SO_2$ ligands. In order to facilitate the study of a wide variety of isomeric structures, we have used the unsubstituted cyclopentadienyl ligand, $\eta^5$-$C_5H_5$, rather than the peralkylated cyclopentadienyl ligand.

## 2. THEORETICAL METHODS

DFT methods have evolved as a practical and effective computational tool, especially for organometallic compounds.[11−17] Three DFT methods were used in this paper. The first method is the hybrid $\omega$B97X-D method, which adds long-range exchange, short-range exact exchange, and empirical dispersion correction to the B97 exchange-correlation functional.[18,19] The second method is the BP86 method using Becke's 1988 exchange functional (B) with Perdew's 1986 gradient-corrected correlation functional (P86).[20,21] The third DFT method used is MPW1PW91. This combines the modified Perdew−Wang exchange functional with the Perdew−Wang 91 correlation functional.[22,23]

Dunning's triple-$\zeta$ (TZ) correlation-consistent basis sets cc-pVTZ, for the hydrogen, carbon, sulfur, and oxygen atoms,[24,25] and cc-pVTZ-



DOI: 10.1021/acs.inorgchem.7b02064
Inorg. Chem. 2017, 56, 14486−14493

PP with relativistic effective core potential (ECP), for the rhodium and iridium atoms,[26,27] were used in the ωB97X-D method. Huzinaga–Dunning's contracted double-ζ (DZ) contraction sets[28−30] were used for the BP86 and MPW1PW91 methods by adding a set of spherical harmonic d polarization functions with orbital exponents $\alpha_d(C)$ = 0.75, $\alpha_d(O)$ = 0.85, and $\alpha_d(S)$ = 0.70 for the carbon, oxygen, and sulfur atoms, as well as a set of p polarization functions, $\alpha_p(H)$ = 0.75, for the hydrogen atoms. The Stuttgart–Dresden ECP plus DZ (SDD) and relativistic ECP basis sets were used for the rhodium and iridium atoms in the BP86 and MPW1PW91 methods.[31]

The geometries of the structures were fully optimized. The vibrational frequencies and the corresponding IR intensities were evaluated analytically. All of the computations were performed using the *Gaussian 09* program.[32] The ultrafine grid (99, 590) for the ωB97X-D method and fine grid (75, 302) for the BP86 and MPW1PW91 methods were used for evaluating integrals numerically. In order to investigate the small imaginary vibrational frequencies, the finer (120, 974) grid was used.[33] These three DFT methods generally predict consistent geometries and relative energies for the present studies. For the sake of brevity, we only report the ωB97X-D/(cc-pVTZ and cc-pVTZ-PP) results in the text. The other results at the BP86 (DZP and SDD) and MPW1PW91/(DZP and SDD) levels are included in the Supporting Information.

## 3. RESULTS AND DISCUSSION

In the present paper, the $Cp_2M_2(SO_2)_2(CH_2)_2$ (M = Rh, Ir) structures are designated as **M-*n***, where **M** stands for the transition metals (Rh or Ir) and ***n*** orders the relative energies of the structures. Thus, **Rh-1** and **Ir-1** denote the lowest-energy $Cp_2Rh_2(SO_2)_2(CH_2)_2$ and $Cp_2Ir_2(SO_2)_2(CH_2)_2$ structures, respectively. Because the energy ordering for the $Cp_2Rh_2(SO_2)_2(CH_2)_2$ structures is not always the same as those for their iridium analogues, **Rh-*n*** and **Ir-*n*** may not always have analogous geometries. For example, the geometry of **Rh-2** corresponds to that of **Ir-3** rather than **Ir-2**.

We have found 24 low-energy $Cp_2M_2(SO_2)_2(CH_2)_2$ (M = Rh, Ir) structures for each metal using the DFT methods. These include structures with separate $SO_2$ ligands as well as structures in which the $SO_2$ groups have coupled to form dithionite or isodithionite $S_2O_4$ ligands. All of the low-energy $Cp_2M_2(SO_2)_2(CH_2)_2$ structures are singlet-state structures. We have also investigated the corresponding triplet-state structures. However, the rhodium and iridium triplet-state structures were found to lie at least ∼28 kcal/mol (M = Rh) or ∼40 kcal/mol (M = Ir) in energy above the corresponding global minima. Thus, only the singlet-state structures are reported in the present paper.

The $Cp_2M_2(SO_2)_2(CH_2)_2$ structures can be classified into three categories. The first structure category has the two $CH_2$ groups coupled to form a coordinated ethylene ligand. The second structure category has the $CH_2$ groups coupled with hydrogen transfer to give a methylcarbene ligand. In these two categories, the two $SO_2$ groups are not coupled and are bonded to one metal atom (for the terminal $SO_2$ groups) or both metal atoms (for the bridging $SO_2$ groups) as separate units exclusively through their sulfur atoms. The third structure category has two $SO_2$ groups coupled to form either a dithionite ($O_2SSO_2$) or an isodithionite ($OSOSO_2$) ligand bridging the central $M_2$ unit through two M–S bonds.

**3.1. $Cp_2M_2(SO_2)_2(C_2H_4)$ Structures Exhibiting Coupling of the Methylene Ligands to a Coordinated Ethylene Ligand.** Most of the $Cp_2M_2(SO_2)_2(CH_2)_2$ (M = Rh, Ir) structures in this category are relatively low-energy structures (Figure 3). The lowest-energy $Cp_2Rh_2(SO_2)_2(CH_2)_2$ structure, **Rh-1**, has two terminal Cp ligands, one terminal $SO_2$ ligand, one bridging $SO_2$ ligand, and one terminal ethylene ligand. The ethylene ligand acts as a π-electron donor, providing two electrons from its π orbital to the "right" rhodium atom in Figure 3. The two $SO_2$ groups are both two-electron donors. The Rh–Rh distance in **Rh-1** of 2.821 Å suggests a formal single bond. Thus, each rhodium atom in **Rh-1** has the favored 18-electron configuration. The lowest-energy $Cp_2Ir_2(SO_2)_2(CH_2)_2$ structure **Ir-1** has a geometry very similar to that of **Rh-1**. The Ir–Ir distance in **Ir-1** of 2.815 Å indicates a formal single bond so that each iridium atom in **Ir-1** also has the favored 18-electron configuration. The cyclopentadienyl rings in **Rh-1** and **Ir-1** have a *trans* configuration around the M–M bond.

Structures **Rh-2** and **Ir-3** have geometries similar to those of **Rh-1** and **Ir-1**, differing only by an internal rotation around the M–M axis (Figure 3). They thus correspond to the *cis* isomers of **Rh-1** and **Ir-1**, respectively. Structures **Rh-2** and **Ir-3** are relatively low-energy structures, lying only 1.7 and 3.1 kcal/mol, respectively, in energy above **Rh-1** and **Ir-1**. Similar to **Rh-1** and **Ir-1**, each metal atom (Rh and Ir) in **Rh-2** and **Ir-3** also has the favored 18-electron configuration.

Structures **Rh-3** and **Rh-5** are another pair of *cis*/*trans* isomers, lying 6.2 and 8.3 kcal/mol, respectively, in energy above **Rh-1** (Figure 3). Different from the **Rh-1**/**Rh-2** pair, the **Rh-3**/**Rh-5** pair has two semibridging $SO_2$ groups, with shorter Rh–S distances of ∼2.2 Å and longer Rh–S distances of 2.4–2.5 Å. The higher energy of structure **Rh-5** relative to **Rh-3** may arise from the steric effect of the closer Cp group adjacent to the two semibridging $SO_2$ groups. The iridium analogues, namely, **Ir-7** and **Ir-8**, have geometries similar to those of **Rh-3** and **Rh-5** and lie 11.5 and 13.6 kcal/mol, respectively, in energy above **Ir-1**. The M–M distances of ∼2.8 Å in these structures correspond to formal single bonds, thereby giving each metal atom the favored 18-electron configuration.

The $C_{2v}$ structures **Rh-6** and **Ir-4** have analogous geometries (Figure 3). Note that structure **Rh-6** has a tiny imaginary vibrational frequency (∼10*i* $cm^{-1}$), which can be removed by using the finer grid (120, 974). Thus, **Rh-6** is confirmed to be a genuine minimum on the potential surface. Structures **Rh-6** and **Ir-4** lie 12.3 and 10.8 kcal/mol, respectively, above their corresponding global minima **M-1** (M = Rh, Ir). Similar to **Rh-3** and **Ir-7**, there are two bridging $SO_2$ groups in **Rh-6** and **Ir-4**. However, unlike **Rh-3** and **Ir-7**, the ethylene ligand in **Rh-6** and **Ir-4** is no longer terminal but bridges the two metal atoms by donating one electron to each metal atom. The M–M distances of ∼2.8 Å in **Rh-6** and **Ir-4** correspond to formal single bonds, thereby giving each metal atom the favored 18-electron configuration.

Another *trans*/*cis*-$Cp_2Rh_2(SO_2)_2(CH_2)_2$ isomer pair **Rh-9**/**Rh-15** has two terminal $SO_2$ groups, with the ethylene ligand bridging the two rhodium atoms (Figure 3). Structures **Rh-9** and **Rh-15** lie 15.5 and 24.0 kcal/mol, respectively, in energy above **Rh-1**. The iridium analogues **Ir-5**/**Ir-18**, lying 11.4 and 21.0 kcal/mol, respectively, in energy above **Ir-1**, have geometries similar to **Rh-9**/**Rh-15**. The M–M distances in these structures of ∼2.7 Å are ∼0.1 Å shorter than the M–M distances in the lower-energy $Cp_2M_2(SO_2)_2(C_2H_4)$ structures with terminal ethylene ligands. However, the M–M distances can still be considered to be formal single bonds, thereby giving each metal atom the favored 18-electron configuration.

The last pair of *trans*/*cis*-$Cp_2Rh_2(SO_2)_2(C_2H_4)$ isomers in this category, namely, **Rh-7** and **Rh-14**, lies 15.0 and 23.4 kcal/mol, respectively, in energy above **Rh-1** (Figure 3). Structures



DOI: 10.1021/acs.inorgchem.7b02064
*Inorg. Chem.* 2017, 56, 14486–14493

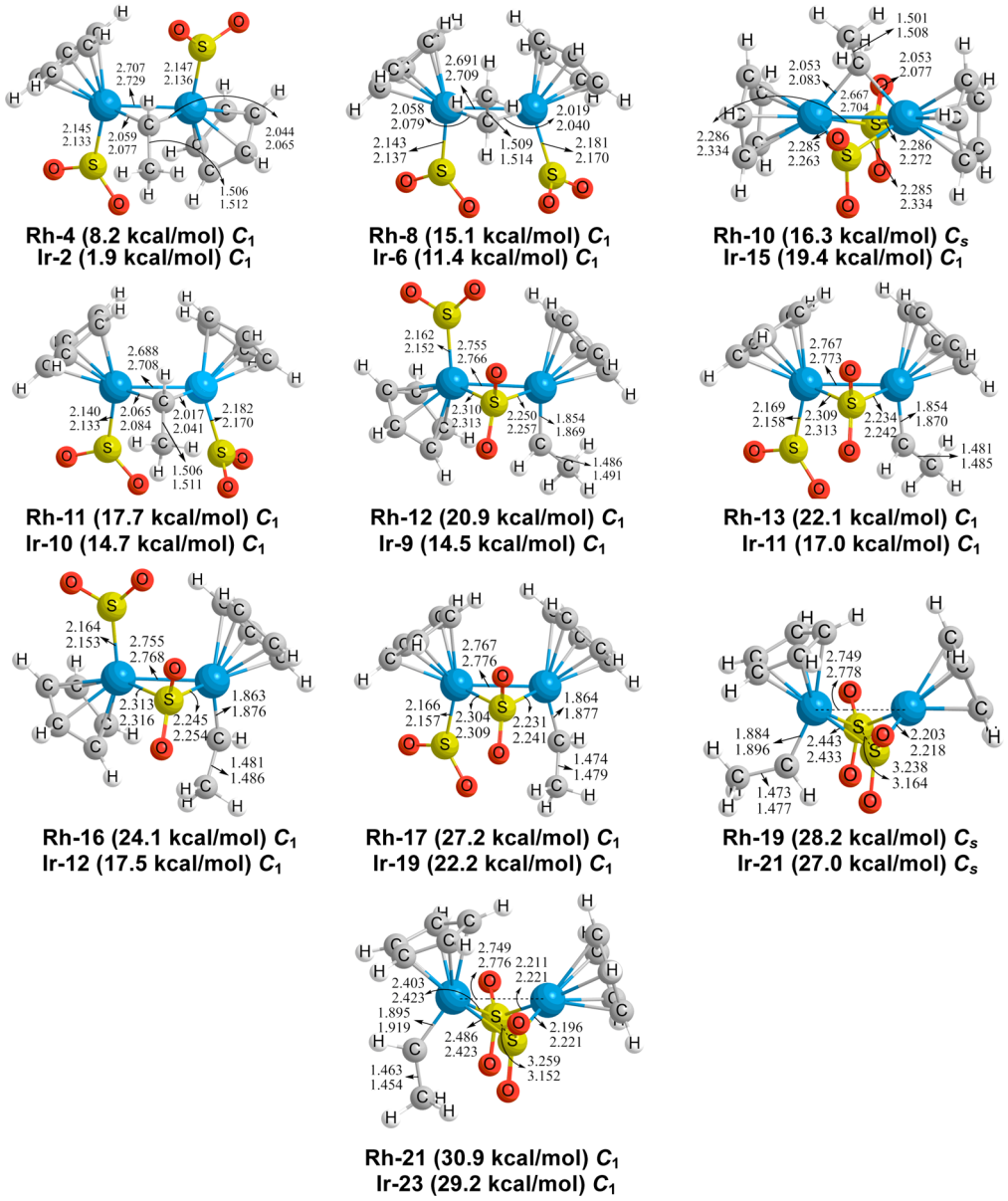


**Figure 4.** $Cp_2M_2(SO_2)_2(CHCH_3)$ (M = Rh, Ir) structures with the coordinated methylcarbene ligands optimized by the $\omega$B97X-D method. The distances (in Å) for M = Rh are on the top, and those for M = Ir are on the bottom.

**Rh-7**/**Rh-14** differ from **Rh-9**/**Rh-15** in the nature of the ethylene bridge between the two $CpRh(SO_2)$ units. Thus, in **Rh-7**/**Rh-14**, the Rh···Rh distances of 4.311 and 4.305 Å, respectively, are too long for a direct Rh−Rh bond. Instead, the two $CpRh(SO_2)$ units are linked by an ethylene ligand perpendicular to the Rh−Rh axis so that the $\pi$ orbital can provide two electrons to each $CpRh(SO_2)$ unit through multicenter $Rh_2C_2$ bonding. As a result, each rhodium atom in **Rh-7** and **Rh-14** still has the favored 18-electron configuration, even with the lack of an Rh−Rh bond. The $Cp_2Ir_2(SO_2)_2(C_2H_4)$ structures **Ir-22** and **Ir-24** have geometries similar to those of **Rh-7** and **Rh-14**, respectively, so their iridium atoms have the favored 18-electron configuration. However, **Ir-22** and **Ir-24** are much higher-energy structures than their rhodium analogues, lying 29.0 and 40.1 kcal/mol, respectively, in energy above **Ir-1**.

### 3.2. $Cp_2M_2(SO_2)_2(CHCH_3)$ Structures Exhibiting Coupling of Coordinated Methylene Followed by Hydrogen Migration to Coordinated Methylcarbene.

A total of 10 $Cp_2M_2(SO_2)_2(CHCH_3)$ (M = Rh, Ir) structures are found to have a methylcarbene ligand (Figure 4). Most of these structures correspond to structures with an ethylene ligand discussed in the previous section. They thus are potentially derived from the ethylene complexes by hydrogen migration within the ethylene ligand to give a methylcarbene ligand. The $Cp_2M_2(SO_2)_2(CHCH_3)$ structures with bridging methylcarbene ligands are of lower energy than those with terminal methylcarbene ligands.

The *trans*/*cis* pair of structures **Rh-12**/**Rh-13** is related to the *trans*/*cis* pair **Rh-1**/**Rh-2**, with two terminal Cp ligands, one terminal $SO_2$ ligand, and one bridging $SO_2$ ligand (Figure 4). However, they are higher-energy structures, with **Rh-12** and **Rh-13** lying 20.9 and 22.1 kcal/mol, respectively, in energy above **Rh-1**. The terminal methylcarbene ligand is a two-electron donor through its carbene carbon atom. The iridium analogues **Ir-9** and **Ir-11**, lying 14.5 and 17.0 kcal/mol,



DOI: 10.1021/acs.inorgchem.7b02064
*Inorg. Chem.* 2017, 56, 14486−14493

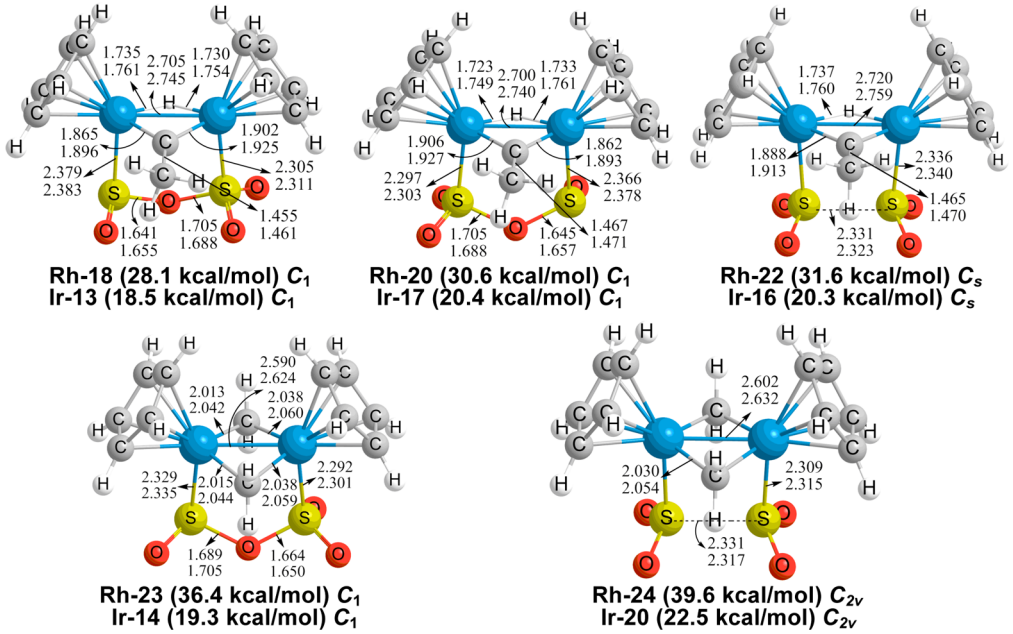


**Figure 5.** $Cp_2M_2(S_2O_4)(CH_2)_2$ (M = Rh, Ir) structures with $SO_2$ coupling to give coordinated dithionite or isodithionite, optimized by the $\omega$B97X-D method. The distances (in Å) for M = Rh are on the top, and those for M = Ir are on the bottom.

respectively, in energy above **Ir-1**, have the same geometries as **Rh-12** and **Rh-13**. The M−M distances of ∼2.8 Å in these complexes correspond to formal single bonds, thereby giving each metal atom the favored 18-electron configuration.

The *trans*/*cis* pair of structures **Rh-16** and **Rh-17**, lying 24.1 and 27.2 kcal/mol, respectively, in energy above **Rh-1**, has geometries very similar to those of **Rh-12** and **Rh-13**, differing only by the orientation of the methylcarbene ligand (Figure 4). The endo pair **Rh-16**/**Rh-17** has higher energies than the exo pair **Rh-12**/**Rh-13** because of the steric effect. The iridium analogues **Ir-12** and **Ir-19**, lying 17.5 and 22.2 kcal/mol, respectively, in energy above **Ir-1**, have essentially the same geometries as **Rh-16** and **Rh-17**. The M−M distances of ∼2.8 Å in these complexes correspond to the formal single bonds required to give each metal atom the favored 18-electron configuration.

Structures **Rh-19** and **Rh-21**, lying 28.2 and 30.9 kcal/mol, respectively, in energy above **Rh-1**, are related to the *cis* structure **Rh-3** by replacing the ethylene ligand with a terminal methylcarbene ligand (Figure 4). Both **Rh-19** and **Rh-21** have *cis* configurations of the Cp rings around the Rh−Rh axis. However, **Rh-21** differs from **Rh-19** in the orientation of the methylcarbene ligand. In addition, structure **Rh-19** has one small imaginary vibrational frequency (<20*i* $cm^{-1}$) and collapses to **Rh-13** after following the corresponding normal mode. The corresponding iridium structures **Ir-21** and **Ir-23** lie 27.0 and 29.2 kcal/mol, respectively, in energy above **Ir-1**. Similar to **Rh-19**, structure **Ir-21** also has one small imaginary vibrational frequency (∼20*i* $cm^{-1}$) and collapses to **Ir-11** after following the corresponding normal mode. The *trans* isomers corresponding to **Rh-19**/**Rh-21** and **Ir-21**/**Ir-23** have high energies (>35 kcal/mol). They are also not local minima because they have one or two large imaginary vibrational frequencies (∼100*i* $cm^{-1}$). They collapse to **Rh-12**/**Rh-16** and **Ir-9**/**Ir-12**, respectively, after, following the corresponding normal modes. The M−M distances of ∼2.8 Å in these structures correspond to the formal single bonds required to give each metal atom the favored 18-electron configuration.

The *trans*/*cis* pair of **Rh-4** and **Rh-8**, lying 8.2 and 15.1 kcal/mol, respectively, in energy above **Rh-1**, is related to **Rh-9** and **Rh-15**, respectively, with a bridging methylcarbene ligand replacing the bridging ethylene ligand (Figure 4). The iridium analogues **Ir-2** and **Ir-6** lie 1.9 and 11.4 kcal/mol, respectively, in energy above **Ir-1**. The methylcarbene ligand in **Rh-4**/**Rh-8** bridges the two rhodium atoms using only the carbene carbon atom, donating its lone-pair electrons. This is different from the bridging ethylene molecule in **Rh-9**/**Rh-15**, in which the ethylene ligand bridges the two rhodium atoms using both carbon atoms, with one carbon atom for each rhodium atom. The M−M distances in these structures of ∼2.7 Å are ∼0.1 Å shorter than the M−M distances in the $Cp_2M_2(SO_2)_2(C_2H_4)$ and $Cp_2M_2(SO_2)_2(CHCH_3)$ structures with terminal hydrocarbon ligands. However, these M−M distances can still be considered formal single bonds, thereby giving each metal atom the favored 18-electron configuration.

Structures **Rh-11** and **Ir-10**, lying 17.7 and 14.7 kcal/mol, respectively, in energy above **Rh-1** and **Ir-1**, are also similar to **Rh-8** and **Ir-6**, differing only by the orientation of the bridging methylcarbene ligand. The Rh−Rh distance in **Rh-11** and the Ir−Ir distance in **Ir-10** are 2.688 and 2.708 Å, respectively, which can still be considered formal single bonds, thereby giving each metal atom the favored 18-electron configuration.

Structure **Rh-10**, lying 16.3 kcal/mol in energy above **Rh-1**, has two bridging $SO_2$ ligands and one bridging methylcarbene ligand (Figure 4). Structure **Rh-10** is thus related to **Rh-6** by replacing the bridging ethylene ligand with a bridging methylcarbene ligand. The M−M distances of ∼2.7 Å in **Rh-10** and **Ir-15** suggest the formal single bonds required to give each metal atom the favored 18-electron configuration. **Rh-10** has $C_s$ symmetry (Figure 4), but the corresponding $C_s$ structure for **Ir-15** has one very small imaginary vibrational frequency (<20*i* $cm^{-1}$). Following the corresponding normal mode to give the $C_1$ minimum for **Ir-15** lowers the energy by only ∼0.02 kcal/mol.

The $Cp_2M_2(SO_2)_2(C_2H_4)$ structures **Rh-7**/**Rh-14** and **Ir-22**/**Ir-24** with a bridging ethylene ligand perpendicular to the M−



DOI: 10.1021/acs.inorgchem.7b02064
*Inorg. Chem.* 2017, 56, 14486−14493

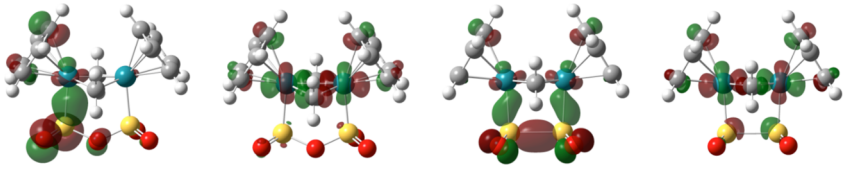


**Figure 6.** Related orbitals (isovalue = 0.05) in the main transition for **Rh-23** and **Rh-24**.

M axis discussed in section 3.1 do not have analogues with a bridging methylcarbene ligand. This is because a methylcarbene ligand cannot donate four electrons to the two metal atoms in the manner of ethylene in **Rh-7**/**Rh-14** and **Ir-22**/**Ir-24**.

**3.3. $Cp_2M_2(S_2O_4)(CH_2)_2$ Structures Exhibiting Coupling of Coordinated $SO_2$.** Five $Cp_2M_2(S_2O_4)(CH_2)_2$ structures are found with the two $SO_2$ ligands coupled to form either a bridging dithionite ($O_2SSO_2$) or a bridging isodithionite ($OSOSO_2$) ligand (Figure 5). The rhodium $Cp_2Rh_2(S_2O_4)(CH_2)_2$ structures are rather high-energy structures, lying 28–40 kcal/mol above **Rh-1**. The corresponding iridium structures $Cp_2Ir_2(S_2O_4)(CH_2)_2$ have more moderate energies, lying 18–23 kcal/mol in energy above **Ir-1**.

The $Cp_2Rh_2(S_2O_4)(CH_2)_2$ structures **Rh-18** and **Rh-20**, lying 28.1 and 30.6 kcal/mol in energy above **Rh-1**, are two stereoisomers, both containing terminal Cp ligands, a bridging isodithionite ($OSOSO_2$) ligand, a bridging three-electron donor methylcarbyne ($CH_3C$) ligand, and a bridging hydride ligand (Figure 5). The $OSOSO_2$ ligand is bonded to each rhodium atom through a sulfur atom and thus is a two-electron donor. The corresponding iridium structures **Ir-13** and **Ir-17** lie 18.5 and 20.4 kcal/mol, respectively, above **Ir-1**. The M–M distances of ~2.7 Å in these structures suggest formal single bonds, thereby giving each metal atom the favored 18-electron configuration.

Structures **Rh-23** and **Ir-14**, lying 36.4 and 19.3 kcal/mol in energy above the corresponding **M-1** structures, have similar geometries with two separate methylene groups bridging the two metal atoms, each acting as a two-electron donor (Figure 5). The isodithionite ($OSOSO_2$) ligand also bridges the two metal atoms as a two-electron donor, with each sulfur atom donating one electron to one metal atom. The M–M distances in **Rh-23** and **Ir-14** are shortened to ~2.6 Å, apparently because of the effect of the two bridging methylene groups. However, the M–M bonds can still be interpreted as formal single bonds to give each metal atom the favored 18-electron configuration.

The two structures **Rh-22** and **Rh-24**, lying 31.6 and 39.6 kcal/mol, respectively, in energy above **Rh-1**, have a bridging dithionite ($O_2SSO_2$) ligand with a long S–S distance (~2.3 Å), which can be considered as a two-electron donor (Figure 5). In **Rh-22**, the two methylene groups couple with hydrogen migration to form a three-electron-donor bridging methylcarbyne ($CH_3C$) ligand and a bridging hydride ligand similar to **Rh-18** and **Rh-20** discussed above. This combination of bridging ligands donates four electrons to the central $Rh_2$ unit. In **Rh-24**, the two methylene groups are not coupled but separately bridge the two rhodium atoms. They also donate a total of four electrons to the central $Rh_2$ unit. The Rh–Rh distance in **Rh-22** is 2.720 Å, which is shortened to 2.602 Å in **Rh-24**, apparently because of the two bridging methylene groups. In both **Rh-22** and **Rh-24**, the Rh–Rh distances suggest the formal single bonds required to give each rhodium atom the favored 18-electron configuration. The Rh–Rh distance of 2.602 Å in **Rh-24** is very close to the experimental value[9] of 2.622 Å in the permethylated derivative $Cp^*_2Rh_2(\mu\text{-}CH_2)_2(S_2O_4)$. The iridium structures **Ir-16** and **Ir-20**, lying 20.3 and 22.5 kcal/mol, respectively, in energy above **Ir-1**, are the analogues of **Rh-22** and **Rh-24**, respectively.

The **Rh-23** and **Rh-24** structures are similar to those in the experimentally observed permethylated photochromic system $Cp^*_2Rh_2(\mu\text{-}CH_2)_2(OSOSO_2)$/$Cp^*_2Rh_2(\mu\text{-}CH_2)_2(S_2O_4)$ ($Cp^* = \eta^5\text{-}Me_5C_5$). We performed time-dependent DFT calculations to examine the excited states of **Rh-23** and **Rh-24** structures at the same level as the structure optimization. The unscaled calculated $\lambda_{max}$ values, both corresponding to the highest occupied molecular orbital (HOMO)–lowest unoccupied molecular orbital (LUMO) transition for the **Rh-23** and **Rh-24** structures, are 415 and 477 nm, respectively. These $\lambda_{max}$ values are close to those of their corresponding experimental permethylated derivative structures, 475 and 510 nm, respectively.[9] Furthermore, we checked the orbitals in the transitions and assigned the absorption as a charge-transfer (CT) band from the $\sigma$(Rh–SO) (HOMO) to the $\sigma^*$(Rh–Rh) (LUMO) orbitals for **Rh-23** and a CT band from the $\sigma$(S–S) and $\sigma$(Rh–S) (HOMO) to the $\sigma^*$(S–S) and $\sigma^*$(Rh–Rh) (LUMO) orbitals for **Rh-24** (Figure 6). These transitions of **Rh-23** and **Rh-24** are also similar to those of their permethylated derivatives.[9] This indicates that the **Rh-23** and **Rh-24** structures can convert to each other through the photochromic process as their permethylated derivatives.

The thermodynamic conversion between **Rh-23** and **Rh-24** was also investigated. The transition-state structure of this conversion was found and confirmed by IRC calculation at the $\omega$B97X-D/cc-pVDZ (for H, C, O, S)[24,25] and cc-pVDZ-PP (including ECP for Rh)[26] levels. The energy barriers for the forward (**Rh-23** to **Rh-24**)/reverse (**Rh-24** to **Rh-23**) reactions of this conversion were found to be 32.3/23.7 kcal/mol. Such high barriers indicate that the thermodynamic conversion would not occur very fast. As reported, the related permethylated derivative of **Rh-23** needs 3 weeks to convert to the permethylated **Rh-24** completely.[7] It can be inferred that the experimentally observed structures **Rh-23** and **Rh-24** need to overcome higher barriers to convert to other isomers after more complicated isomerizations. Therefore, they can be kinetically stable due to the high isomerization barrier.

## 4. CONCLUSIONS

The potential energy surfaces for the $Cp_2M_2(CH_2)_2(SO_2)_2$ (M = Rh, Ir) systems predict isomers arising from two possible ligands that can couple, namely, methylene units coupling to form an ethylene ligand and $SO_2$ coupling to form a dithionite ligand. Furthermore, hydrogen migration can occur in ethylene ligands ($CH_2CH_2$) to form methylcarbene ligands ($CH_3CH$).



DOI: 10.1021/acs.inorgchem.7b02064
Inorg. Chem. 2017, 56, 14486–14493

Similarly, dithionite ligands ($O_2SSO_2$) are predicted to isomerize to give isodithionite ligands ($O_2SOSO$). This last process well describes what occurs in the experimentally observed[7,8] photoconversion of $Cp^*_2Rh_2(\mu\text{-}CH_2)_2(\mu\text{-}O_2SSO_2)$ to the isodithionite complex $Cp^*_2Rh(\mu\text{-}CH_2)_2(\mu\text{-}O_2SOSO)$. Finally ethylene, methylcarbene, and $SO_2$ can function as either terminal or bridging ligands. However, the dithionite and isodithionite ligands are only found in bridging positions in the low-energy structures.

The lowest-energy structures for the $Cp_2M_2(CH_2)_2(SO_2)_2$ (M = Rh, Ir) systems are predicted to be the $Cp_2M_2(CH_2CH_2)(SO_2)_2$ structures with separate $SO_2$ ligands but with coupling of the methylene groups to give an ethylene ligand (Figure 3). We find that next comes the $Cp_2M_2(CH_3CH)(SO_2)_2$ structures in which hydrogen migration has occurred to convert the ethylene ligand into a methylcarbene ligand (Figure 4). Among this group of structures, those with bridging methylcarbene ligands are energetically preferred over those with terminal methylcarbene ligands. Structures in which the two $SO_2$ units have coupled to form a dithionite or isodithionite ligand (Figure 5) are predicted to be the highest-energy structures. These structures with a dithionite or isothionite ligand include $Cp_2M_2(\mu\text{-}H)(\mu\text{-}CH_3C)(\mu\text{-}S_2O_4)$ structures in which the $M_2$ unit has formally inserted into a C−H bond of a methylcarbene ligand to give separate bridging hydride and bridging methylcarbyne ligands.

The limited known experimental chemistry of these systems involves dithionite and isodithionite structures that are relatively high-energy structures related to **Rh-24**/**Ir-20** and **Rh-23**/**Ir-14**, respectively (Figure 5). These structures, predicted here to be high-energy structures, are clearly kinetically favored $Cp^*_2Rh_2(CH_2)_2(S_2O_4)$ structures, with the two bridging $CH_2$ ligands and one bridging $S_2O_4$ ligand reflecting the method of synthesis rather than the thermodynamically favored lowest-energy structure with a terminal $CH_2CH_2$ ligand and two separate $SO_2$ units. Formation of these high-energy isomers occurs because the entry into the experimental chemistry uses the $Cp^*_2Rh_2(CH_2)_2(S_2O_4)$ isomer obtained from the metathesis of $Cp^*_2Rh_2(\mu\text{-}CH_2)_2(\mu\text{-}Cl)_2$ with sodium dithionite. The use of dithionite in the synthesis of these species starts with coupled $SO_2$ groups and thus selectively leads initially to a kinetically favored relatively high-energy structure related to **Rh-24** with an intact bridging dithionite ligand. The relatively high isomerization barrier (>20 kcal/mol) kinetically stabilizes both experimentally related isomers as viable species that can be individually structurally characterized by X-ray crystallography.

Synthesis of the lower-energy $Cp^*_2Rh_2(CH_2)_2(SO_2)_2$ isomers with separate $SO_2$ ligands should be feasible using the reaction of free $SO_2$ with a more highly reduced rhodium species such as $Cp^*_2Rh_2(CH_2)_2$. However, this $Cp^*_2Rh_2(CH_2)_2$ precursor supposedly obtained from the sodium metal reduction of $Cp^*_2Rh_2(\mu\text{-}CH_2)_2(\mu\text{-}Cl)_2$ is in the literature only as a claim in a Japanese patent.[34] It is not clear from the literature whether $Cp^*_2Rh_2(CH_2)_2$ has actually been synthesized or is described in the patent only to broaden its scope. However, the iridium analogue $Cp^*_2Ir_2(CH_2)_2$ has been reported.[35] Hopefully, our prediction of lower-energy $Cp^*_2Rh_2(CH_2)_2(SO_2)_2$ isomers than the currently known dithionite and isodithionite isomers will stimulate successful experimental efforts to synthesize $Cp^*_2Rh_2(CH_2)_2$ and study its reaction with $SO_2$.

## ■ ASSOCIATED CONTENT

### Supporting Information

The Supporting Information is available free of charge on the ACS Publications website at DOI: 10.1021/acs.inorgchem.7b02064.

Cartesian coordinates and total energies of the optimized $Cp_2M_2(SO_2)_2(CH_2)_2$ (M = Rh, Ir) structures by the ωB97X-D, MPW1PW91, and BP86 methods (Tables S1−S96), harmonic vibrational frequencies and corresponding IR intensities predicted for the $Cp_2M_2(SO_2)_2(CH_2)_2$ (M = Rh, Ir) structures by the ωB97X-D, MPW1PW91, and BP86 methods (Tables S97−S102), and the complete *Gaussian 09* reference (ref 32) (PDF)

## ■ AUTHOR INFORMATION


### Corresponding Authors

*E-mail: luoqiong@scnu.edu.cn (Q.L.).
*E-mail: rbking@chem.uga.edu (R.B.K.).

### ORCID

R. Bruce King: 0000-0001-9177-5220
Henry F. Schaefer: 0000-0003-0252-2083


### Author Contributions

[§]D.R. and S.G. contributed equally to this work.

### Notes

The authors declare no competing financial interest.

## ■ ACKNOWLEDGMENTS

We are indebted to the National Natural Science Foundation of China (21573079 and 21673084), the Training Plan of Guangdong Province Outstanding Young Teachers in Higher Education Institutions (HS20150003), and the Special Program for Applied Research on Super Computation of the NSFC-Guangdong Joint Fund (the second phase), the China Postdoctoral Science Foundation (2016M602093), the Shandong Postdoctoral Innovation Project (201603065), and the Qingdao Postdoctoral Application Research Project (2016006) for support of this research in China. In addition, we acknowledge support from the U.S. National Science Foundation (Grants CHE-1057466 and CHE-1661604).

## ■ REFERENCES


(1) Kubas, G. J. Chemical transformations and facile disproportionation of sulfur dioxide on transition metal complexes. *Acc. Chem. Res.* **1994**, *27*, 183−190.

(2) Mews, R.; Lork, E.; Watson, P. G.; Görtler, B. Coordination chemistry in and of sulfur dioxide. *Coord. Chem. Rev.* **2000**, *197*, 277−320.

(3) Kovalevsky, A. Y.; Bagley, K. A.; Cole, J. M.; Coppens, P. Light-induced metastable linkage isomers of ruthenium sulfur dioxide complexes. *Inorg. Chem.* **2003**, *42*, 140−147.

(4) Bowes, K. F.; Cole, J. M.; Husheer, S. L. G.; Raithby, P. R.; Savarese, T. L.; Sparkes, H. A.; Teat, S. J.; Warren, J. E. Photocrystallographic structure determination of a new geometric isomer of $[Ru(NH_3)_4(H_2O)(\eta^1\text{-}OSO)][MeC_6H_4SO_3]_2$. *Chem. Commun.* **2006**, 2448−2450.

(5) Dunitz, J. D. The structure of sodium dithionite and the nature of the dithionite ion. *Acta Crystallogr.* **1956**, *9*, 579−586.

(6) Weinrach, J. B.; Meyer, D. R.; Guy, J. T., Jr.; Michalski, P. E.; Carter, K. L.; Grubisha, D. S.; Bennett, D. W. A structural study of sodium dithionite and its ephemeral dihydrate: A new conformation for the dithionite ion. *J. Crystallogr. Spectrosc. Res.* **1992**, *22*, 291−301.




DOI: 10.1021/acs.inorgchem.7b02064
*Inorg. Chem.* 2017, 56, 14486−14493

(7) Nakai, H.; Mizuno, M.; Nishioka, T.; Koga, N.; Shiomi, K.; Miyano, Y.; Irie, M.; Breedlove, B. K.; Kinoshita, I.; Hayashi, Y.; Ozawa, Y.; Yonezawa, T.; Toriumi, K.; Isobe, K. Direct observation of photochromic dynamics in the crystalline state of an organorhodium dithionite complex. *Angew. Chem., Int. Ed.* **2006**, *45*, 6473−6476.
(8) Miyano, Y.; Nakai, H.; Hayashi, Y.; Isobe, K. Synthesis and structural characterization of a photoresponsive organodirhodium complex with active S−S bonds:$[(Cp^{Ph}Rh)_2(\mu\text{-}CH_2)_2\ (\mu\text{-}O_2SSO_2)]$ ($Cp^{Ph}$= $\eta^5$-$C_5Me_4Ph$). *J. Organomet. Chem.* **2007**, *692*, 122−128.
(9) Nakai, H.; Nonaka, T.; Miyano, Y.; Mizuno, M.; Ozawa, Y.; Toriumi, K.; Koga, N.; Nishioka, T.; Irie, M.; Isobe, K. Photochromism of an organorhodium dithionite complex in the crystalline-state: Molecular motion of pentamethylcyclopentadienyl ligands coupled to atom rearrangement in a dithionite ligand. *J. Am. Chem. Soc.* **2008**, *130*, 17836−17845.
(10) Nakai, H.; Uemura, S.; Miyano, Y.; Mizuno, M.; Irie, M.; Isobe, K. Photoreactivity of crystals of a rhodium dithionite complex with ethyltetramethylcyclopentadienyl ligands: Crystal surface morphology changes and degradation. *Dalton Trans.* **2011**, *40*, 2177−2179.
(11) Ziegler, T.; Autschbach, J. Theoretical methods of potential use for studies of inorganic reaction mechanisms. *Chem. Rev.* **2005**, *105*, 2695−2722.
(12) Bühl, M.; Kabrede, H. Geometries of transition-metal complexes from density-functional theory. *J. Chem. Theory Comput.* **2006**, *2*, 1282−1290.
(13) Brynda, M.; Gagliardi, L.; Widmark, P. O.; Power, P. P.; Roos, B. O. A quantum chemical study of the quintuple bond between two chromium centers in [PhCrCrPh]: *trans*-Bent versus linear geometry. *Angew. Chem., Int. Ed.* **2006**, *45*, 3804−3807.
(14) Sieffert, N.; Bühl, M. Hydrogen generation from alcohols catalyzed by ruthenium−triphenylphosphine complexes: Multiple reaction pathways. *J. Am. Chem. Soc.* **2010**, *132*, 8056−8070.
(15) Schyman, P.; Lai, W.; Chen, H.; Wang, Y.; Shaik, S. The directive of the protein: How does cytochrome P450 select the mechanism of dopamine formation? *J. Am. Chem. Soc.* **2011**, *133*, 7977−7984.
(16) Adams, R. D.; Pearl, W. C.; Wong, Y. O.; Zhang, Q.; Hall, M. B.; Walensky, J. R. Tetrarhena-heterocycle from the palladium-catalyzed dimerization of $Re_2(CO)_8(\mu\text{-}SbPh_2)(\mu\text{-}H)$ exhibits an unusual host−guest behavior. *J. Am. Chem. Soc.* **2011**, *133*, 12994−12997.
(17) Lonsdale, R.; Olah, J.; Mulholland, A. J.; Harvey, J. N. Does compound I vary significantly between isoforms of cytochrome P450? *J. Am. Chem. Soc.* **2011**, *133*, 15464−15474.
(18) Becke, A. D. Density-functional thermochemistry. V. Systematic optimization of exchange-correlation functionals. *J. Chem. Phys.* **1997**, *107*, 8554−8560.
(19) Chai, J. D.; Head-Gordon, M. Long-range corrected hybrid density functionals with damped atom−atom dispersion corrections. *Phys. Chem. Chem. Phys.* **2008**, *10*, 6615−6620.
(20) Becke, A. D. Density-functional exchange-energy approximation with correct asymptotic behavior. *Phys. Rev. A: At., Mol., Opt. Phys.* **1988**, *38*, 3098−3100.
(21) Perdew, J. P. Density-functional approximation for the correlation energy of the inhomogeneous electron gas. *Phys. Rev. B: Condens. Matter Mater. Phys.* **1986**, *33*, 8822−8824.
(22) Adamo, C.; Barone, V. Exchange functionals with improved long-range behavior and adiabatic connection methods without adjustable parameters: The *m*PW and *m*PW1PW models. *J. Chem. Phys.* **1998**, *108*, 664−675.
(23) Zhao, Y.; Pu, J.; Lynch, B. J.; Truhlar, D. G. Tests of second-generation and third-generation density functionals for thermochemical kinetics. *Phys. Chem. Chem. Phys.* **2004**, *6*, 673−676.
(24) Dunning, T. H. Gaussian basis sets for use in correlated molecular calculations. I. The atoms boron through neon and hydrogen. *J. Chem. Phys.* **1989**, *90*, 1007−1023.
(25) Woon, D. E.; Dunning, T. H. Gaussian basis sets for use in correlated molecular calculations. III. The atoms aluminum through argon. *J. Chem. Phys.* **1993**, *98*, 1358−1371.
(26) Peterson, K. A.; Figgen, D.; Dolg, M.; Stoll, H. Energy-consistent relativistic pseudopotentials and correlation consistent basis sets for the 4d elements Y−Pd. *J. Chem. Phys.* **2007**, *126*, 124101.
(27) Figgen, D.; Peterson, K. A.; Dolg, M.; Stoll, H. Energy-consistent pseudopotentials and correlation consistent basis sets for the 5d elements Hf−Pt. *J. Chem. Phys.* **2009**, *130*, 164108.
(28) Huzinaga, S. Gaussian-type functions for polyatomic systems. I. *J. Chem. Phys.* **1965**, *42*, 1293−1302.
(29) Dunning, T. H. Gaussian basis functions for use in molecular calculations. I. Contraction of (9s5p) atomic basis sets for the first-row atoms. *J. Chem. Phys.* **1970**, *53*, 2823−2833.
(30) Dunning, T. H.; Hay, P. J. In *Methods of Electronic Structure Theory*; Schaefer, H. F., Ed.; Plenum Press: New York, 1977; pp 1−27.
(31) Andrae, D.; Häußermann, U.; Dolg, M.; Stoll, H.; Preuß, H. Energy-adjusted *ab initio* pseudopotentials for the second and third row transition elements. *Theor. Chim. Acta* **1990**, *77*, 123−141.
(32) Frisch, M. J.; et al. *Gaussian 09*, revision B.01; Gaussian, Inc.: Wallingford, CT, 2010 (see the Supporting Information for details).
(33) Papas, B. N.; Schaefer, H. F. Concerning the precision of standard density functional programs: Gaussian, Molpro, NWChem, Q-Chem, and Gamess. *J. Mol. Struct.: THEOCHEM* **2006**, *768*, 175−181.
(34) Nakai, H.; Isobe, K.; Nakano, S. Japanese Patent 2008214278.
(35) Nakai, H.; Nakano, S.; Imai, S.; Isobe, K. Extraction of hydrogen from alcohols by a methylene-bridged iridium(I) dinuclear complex having a short Ir−Ir double bond. *Organometallics* **2010**, *29*, 4210−4212.



DOI: 10.1021/acs.inorgchem.7b02064
*Inorg. Chem.* 2017, 56, 14486−14493